AGU PUBLICATIONS

JGR

Journal of Geophysical Research: Space Physics

TECHNICAL REPORTS: METHODS

10.1002/2017JA024153

Key Points:
- A new data analysis tool is introduced to highlight the nonstationarity and nonlinearity characteristics of a signal
- New data analysis tool able to identify intervals in which the signal is Gaussian or leptokurtic in different intermittency conditions
- Comparison scale by scale between statistical analysis of a radio scintillation signal produced by ALIF and by Discrete Wavelet Transform

Correspondence to:
M. Piersanti,
mirko.piersanti@aquila.infn.it

Citation:
Materassi, M., Piersanti, M., Cicone, A., Spogli, L., Zhou, H., & Ezquer, R. G. (2018). Adaptive local iterative for the analysis of nonstationary signals. *Journal of Geophysical Research: Space Physics*, *123*, 1031–1046. https://doi.org/10.1002/2017JA024153

Received 15 MAR 2017
Accepted 13 DEC 2017
Accepted article online 20 DEC 2017
Published online 9 JAN 2018

©2017. American Geophysical Union. All Rights Reserved.

Adaptive Local Iterative Filtering: A Promising Technique for the Analysis of Nonstationary Signals

M. Piersanti[1,2], M. Materassi[3], A. Cicone[4,5], L. Spogli[6,7], H. Zhou[8], and R. G. Ezquer[9,10,11]

[1]Department of Physical and Chemical Sciences, University of L'Aquila, L'Aquila, Italy, [2]Consorzio Area di Ricerca in Astrogeofisica, University of L'Aquila, L'Aquila, Italy, [3]Institute for Complex Systems ISC-CNR, National Research Council, Rome, Italy, [4]DISIM, Universitá degli Studi dell'Aquila, L'Aquila, Italy, [5]Istituto Nazionale di Alta Matematica, Rome, Italy, [6]Istituto Nazionale di Geofisica e Vulcanoligia, Rome, Italy, [7]SpacEarth Technology, Rome, Italy, [8]School of Mathematics, Georgia Institute of Technology, Atlanta, GA, USA, [9]Laboratorio de Ionósfera, Departamento de Física, FACET, Universidad Nacional de Tucumán, Tucumán, Argentina, [10]CIASUR, Facultad Regional Tucumán, Universidad Tecnológica Nacional, Tucumán, Argentina, [11]Consejo Nacional de Investigaciones Científicas y Técnicas, Buenos Aires, Argentina

Abstract Many real-life signals and, in particular, in the space physics domain, exhibit variations across different temporal scales. Hence, their statistical momenta may depend on the time scale at which the signal is studied. To identify and quantify such variations, a time-frequency analysis has to be performed on these signals. The dependence of the statistical properties of a signal fluctuation on the space and time scales is the distinctive character of systems with nonlinear couplings among different modes. Hence, assessing how the statistics of signal fluctuations vary with scale will be of help in understanding the corresponding multiscale statistics of such dynamics. This paper presents a new multiscale data analysis technique, the adaptive local iterative filtering (ALIF), which allows to describe the multiscale nature of the geophysical signal studied better than via Fourier transform, and improves scale resolution with respect to discrete wavelet transform. The example of geophysical signal, to which ALIF has been applied, is ionospheric radio power scintillation on L band. ALIF appears to be a promising technique to study the small-scale structures of radio scintillation due to ionospheric turbulence.

1. Introduction

Many signals in the space physics domain are nonstationary and they exhibit variations across different scales. Such variations are determined by the complexity and nonlinearity of the system that generated them. As a consequence their statistical momenta depend on time and/or space. To identify and quantify such variations, a time-frequency analysis has to be performed on these signals. Clearly, the standard Fourier spectral analysis cannot work in this context since it is not capable to capture nonstationarity. For this reason other techniques have been used extensively in the last decades, like short time Fourier transform, continuous and discrete wavelet transform, Wigner-Ville transform, and similar methods, which allow deriving a time-frequency analysis that capture such variations. However, all these methods suffer of either limited resolution, due to the uncertainty principle studied by Cohen (2001), or interferences in the time-frequency plane (Flandrin, 1998) and require some further processing of the representation. In this line of research some techniques have been proposed in the last years, like the synchrosqueezed wavelet transform (Daubechies & Maes, 1996; Daubechies et al., 2011), the short time Fourier Transform Synchrosqueezing (Thakur & Wu, 2011), etc. Another way to overcome these limitations was proposed in 1998 by Huang and his research group at NASA who developed a new technique, first of its kind, called empirical mode decomposition (EMD) (Huang et al., 1998). The key idea behind this method is a divide et impera approach, which allows overcoming the limitations in the time-frequency representation. In fact, EMD first decomposes a signal into several intrinsic mode components (IMCs), which are functions oscillating around zero, but not necessarily with constant frequencies. We point out that in the literature the IMCs are called intrinsic mode functions (IMFs). However, to avoid confusions with interplanetary magnetic field (IMF), we choose to rename them into IMCs. Then, it performs a time analysis on each component separately. This approach allows eliminating the problems due to both the uncertainty principle and the interferences. However, the EMD technique has proven to be unstable to small perturbations of the initial data. To overcome this issue, Wu and Huang (2009) developed the ensemble empirical mode decomposition (EEMD), where random perturbations with zero averages are artificially added to the original signal.

Each perturbed signal is studied using the EMD algorithm. The outcome of the method is taken to be the mean out of all the decompositions. Both EMD and EEMD lack a rigorous proof of their convergence. Therefore, in the last years several research groups started working for the development of alternative techniques for the decomposition of nonstationary signals. The algorithms developed so far belong to two groups: (1) methods based on optimization and (2) methods based on iteration. Among the first group, we mention the sparse time-frequency representation (Hou et al., 2009), the empirical wavelet transform (Gilles, 2013), and the higher-order structure function technique (Uritsky et al., 2011). All these algorithms require the a priori selection of a suitable basis for the decomposition. Methods based on iteration, instead, are only two: the EMD (and the EEMD), and the iterative filtering (IF) technique (Cicone et al., 2016b, 2017; Lin et al., 2009) with its generalization, the adaptive local iterative filtering (ALIF) (Cicone et al., 2016a). Unlike all the techniques based on optimization, such methods do not require any initial assumption on the signal. Therefore, they produce decompositions that are completely data driven. Furthermore, both IF and ALIF algorithm have a structure which allows for a rigorous analysis of their convergence. In particular, for the IF method mild sufficient conditions that ensure the convergence are known (Cicone et al., 2016a; Wang & Zhou, 2013). Whereas on the convergence and stability analysis of the ALIF algorithm, only promising results exist (Cicone et al., 2016a).

This paper presents ALIF algorithm and the results obtained applying it, as an example, to artificial and real-life ionospheric radio power scintillation signal.

2. Adaptive Local Iterative Filtering

We start presenting EMD algorithm and its structure. Then we show how ALIF stems from it.

The EMD method (Huang et al., 1998), is based on the so-called *sifting process*. Starting with the given signal $s(t)$, the method computes a moving average as the local average between an upper and lower envelopes of $s(t)$. Huang and his collaborators proposed to use cubic splines connecting maxima and minima of the signal to compute the two envelopes. If $\mathcal{M}$ is defined to be the operator capturing the moving average of $s(t)$, then $\mathcal{L}(s)(t) = s(t) - \mathcal{M}(s)(t)$ is an operator capturing the fluctuation part of the signal. The process can be iterated many times considering the fluctuation part as a new signal. Therefore, the first IMC produced by the sifting process is given by

$$g_1^{(\mathrm{EMD})}(t) = \lim_{n\to\infty} \mathcal{L}_{1,n}\left(s_n\right)(t) \tag{1}$$

where $s_n(t) = \mathcal{L}_{1,n-1}(s_{n-1})(t)$, $s_1(t) = s(t)$, and the subscripts in $\mathcal{L}$ stand for the IMC number and the step in the iterative process.

Here the limit is reached at a finite step $N \in \mathbb{N}$ if the moving average $\mathcal{M}_{1,N}(s_N)(t)$ is zero everywhere.

The second IMC is obtained by reapplying the previously defined iterative process to the remainder $r(t) = s(t) - g_1(t)$.

In the same way all the subsequent IMCs can be produced. In particular,

$$g_k^{(\mathrm{EMD})}(t) = \lim_{n\to\infty} \mathcal{L}_{k,n}(r_n)(t) \tag{2}$$

where $r_n(t) = \mathcal{L}_{k,n-1}(r_{n-1})(t)$ and $r_1(t) = r(t)$, which is the remainder $s(t) - g_1^{(\mathrm{EMD})}(t) - \ldots - g_{k-1}^{(\mathrm{EMD})}(t)$. The iterative process stops when $r(t) = s(t) - g_1^{(\mathrm{EMD})}(t) - g_2^{(\mathrm{EMD})}(t) - \ldots - g_m^{(\mathrm{EMD})}(t)$ becomes a trend signal, which means it has at most one local maximum or minimum. The original signal is decomposed as

$$s(t) = \sum_{j=1}^{m} g_j^{(\mathrm{EMD})}(t) + r(t). \tag{3}$$

This method is simple and intuitive, however, as explained in section 1, it has been proven to be unstable in presence of noise due to cubic splines that are used repeatedly in the iterations (Wu & Huang, 2009). Such instability has been overcome with the development of the EEMD algorithm by Wu and Huang (2009). However, despite the proven usefulness of the EEMD method, its mathematical understanding is still very sketchy, and it is still unclear if there will be any improvement in this direction in the upcoming future.

For this reason, Lin et al. (2009) proposed IF method that has been recently further developed into ALIF (Cicone et al., 2016a).

The key idea in both methods is to use the same algorithm framework as the original EMD, but to compute the moving average of a signal $s(t)$, in a different way: as the local integral of $s(t)$ weighted using any low-pass filter/mask $h_n^{(t)}(x)$ compactly supported on $[-l_n(t), l_n(t)]$, where $l_n(t)$ is called the *mask length* which varies with t. As an example we can consider $h_n^{(t)}(x) = a_n^{(t)}(x)$, which is the double ramp given by

$$a_n^{(t)}(x) = \frac{l_n^{(t)} - |x|}{(l_n^{(t)})^2}, \quad x \in [-l_n^{(t)}, l_n^{(t)}]. \tag{4}$$

In Cicone et al. (2016a) the authors suggest to use as a mask in ALIF the so-called Fokker-Planck filters, which have the nice properties of being compactly supported and infinitely smooth on the entire real line. Following their suggestion, for all the decomposition produced with ALIF and shown in this work, we use a Fokker-Planck filter with $\alpha = 0.005$ and $\beta = 0.09$. For further details on this kind of filters we refer the interested reader to Cicone et al. (2016a).

The pseudocode of ALIF is given in Algorithm 1.

Algorithm 1 ALIF Algorithm IMC = ALIF(s)

```
IMC = { }
while the number of extrema of s ≥ 2 do
  s_1 = s
  while the stopping criterion is not satisfied do
    compute the mask length l_n(t) for s_n(t)
    s_{n+1}(t) = s_n(t) − ∫_{−l_n(t)}^{l_n(t)} s_n(t + x) h_n^{(t)}(x) dx
    n = n + 1
  end while
  IMC = IMC ∪ {s_n}
  s = s − s_n
end while
IMC = IMC ∪ {s}
```

As for the EMD technique, two operators can be defined: one capturing the moving average of the signal under study, $\mathcal{M}_{h_n,l_n}(s)(t) = \int_{-l_n(t)}^{l_n(t)} s(t+x) h_n^{(t)}(x) \mathrm{d}x$, and the other doing the same for its fluctuation part, $\mathcal{L}_{h_n,l_n}(s)(t) = s(t) - \mathcal{M}_{h_n,l_n}(s)(t)$. The kth IMC, $k \in \mathbb{N}$, is given by the limit

$$g_k^{(\mathrm{ALIF})}(t) = \lim_{n\to\infty} \mathcal{L}_{h_n,l_n}(r)(t) \tag{5}$$

where $r(t) = s(t) - g_1^{(\mathrm{ALIF})}(t) - g_2^{(\mathrm{ALIF})}(t) - \ldots - g_{k-1}^{(\mathrm{ALIF})}(t)$.

In practical applications of Algorithm 1, n is not allowed to go to infinity; instead, a stopping criterion is used. First $g_{1,n}^{(\mathrm{ALIF})} = \mathcal{L}_{1,n}(s)$ is defined, where $\mathcal{L}_{1,n}$ denotes the operator used in the nth step of the first inner while loop. We define then

$$\mathrm{SD} := \frac{\|g_{1,n}^{(\mathrm{ALIF})} - g_{1,n-1}^{(\mathrm{ALIF})}\|_2}{\|g_{1,n-1}^{(\mathrm{ALIF})}\|_2}. \tag{6}$$

As suggested in Huang et al. (1998) and Lin et al. (2009), the process can be stopped when the value SD reaches a certain threshold or a limit on the maximal number of iterations for each inner while loop can be introduced.

The mask length $l_n(t)$ selection is a crucial step in ALIF. The key idea is to let the algorithm automatically select $l_n(t)$ simply based on local information of the signal under study, for instance, the relative distance between subsequent extrema of the signal. In doing so, the method becomes nonlinear. In fact, given two signals s_1 and s_2, which we assume to have the same number $N \in \mathbb{N}$ of IMCs in their decomposition, in general, $\mathrm{IMC}_{s_1} + \mathrm{IMC}_{s_2} \neq \mathrm{IMC}_{s_1+s_2}$. The number of IMCs in $\mathrm{IMC}_{s_1+s_2}$ could even differ from N.

If the mask length $l_n(t)$ is kept constant over t, the method reduces to the so-called IF algorithm and the moving average computation reduces to the convolution of the signal with the chosen filter.

The IF method has been proven to be a priori convergent under mild conditions on the chosen filter and its limit value is given by an explicit formula for both the continuous and the discrete case in one- and

Table 1
Comparisons of Alternative Techniques for the Time-Frequency Analysis of a Nonstationary Signal

	Fourier	Wavelet	EEMD	ALIF
Basis selection	a priori	a priori	a posteriori adaptive	a posteriori adaptive
Frequency	convolution over global domain, uncertainty	convolution over global domain, uncertainty	differentiation over local domain, certainty	differentiation over local domain, certainty
Nonlinearity	no	no	yes	yes
Nonstationarity	standard, no; short time, yes	yes	yes	yes
Feature extraction	no	discrete, no; continuous, yes	yes	yes
Theoretical base	complete mathematical theory	complete mathematical theory	empirical	partial mathematical theory
Fast algorithm	yes	yes	no	yes

higher-dimensional settings (Cicone et al., 2016a, 2017; Lin et al., 2009; Wang & Zhou, 2013). As shown by Cicone et al. (2016a), IF is also stable under perturbations. The a priori convergence and stability of its generalization, ALIF, is still an open problem in Mathematics. However, ALIF can be already used to decompose general nonstationary and nonlinear signals. In fact, its stability and convergence can be always and easily certified a posteriori every time the algorithm is applied to decompose a signal. In Table 1, we summarize the main features of ALIF compared with other well-known techniques: Fourier, Wavelets, and EEMD. It is clear from this table that ALIF inherits all the good properties of the previously developed methods summarizing them in a single technique, but adding a very important feature: the mathematical background lying below.

3. Discrete Wavelet Transform: A Telegraphic Resume

Discrete wavelet transform (DWT) is a well-known, widely adopted technique (Mallat, 1998; Van den Berg, 1999). In this technique, time series are decomposed along orthonormal functions $f_{l,\tau}(t)$ with scale l and "centered" in $t=\tau$. The DWT coefficient

$$c_{l,\tau} = \int_l w_{\text{det}}(t)\, f^*_{l,\tau}(t)\, \mathrm{d}t \tag{7}$$

describes the contribution of the scale l to the signal w_{det} around $t=\tau$ along the time interval l (Farge, 1992). In turn, the signal $w_{\text{det}}(t)$ reads

$$w_{\text{det}}(t) = \sum_{l,\tau} c_{l,\tau} f_{l,\tau}(t)\,, \tag{8}$$

as long as the set $f_{l,\tau}$ is an orthonormal basis in $L_2(I,\mathbb{C})$, $\left(f_{l',\tau'}, f_{l,\tau}\right) = \delta_{l,l'}\delta_{\tau,\tau'}$: the decomposition hence separates $w_{\text{det}}(t)$ into linearly independent components. This orthogonality condition can only be matched as

$$l_m = \tfrac{L}{2^m},\ m \in \mathbb{N}, \tag{9}$$

being L the total length of the interval I. The mth scale in the set (9) has 2^m points $\tau_{m,1}, \ldots, \tau_{m,2^m}$ in which the 2^m basis elements $f_{l_m,\tau}$ are centered: for example, there will be two τ's for l_1, four τ's for l_2, eight τ's for l_3, and so on. This kind of basis $\left\{f_{l_1,\tau_{1,1}}, f_{l_1,\tau_{1,2}}, f_{l_2,\tau_{2,1}}, f_{l_2,\tau_{2,2}}, f_{l_2,\tau_{2,3}}, f_{l_2,\tau_{2,4}}, \ldots, f_{l_m,\tau_{m,1}}, \ldots, f_{l_m,\tau_{m,2^m}}, \ldots\right\}$ is referred to as *dyadic basis*. Clearly, the higher is m, the shorter is l_m: in data analysis the highest possible m corresponds to $l_{\min} = 2\Delta t$, being Δt the sampling time.

In practice, the total l contribution to $w_{\text{det}}(t)$ can be defined as

$$g_l^{(\text{DWT})}(t) = \sum_{\tau} c_{l,\tau} f_{l,\tau}(t)\,. \tag{10}$$

4. Example of Application: Artificial Signal

We start by applying the proposed ALIF method to an artificial signal, perturbed with red noise, and we compare the resulting decomposition with the ones obtained by EEMD and DWT. We also compare the time

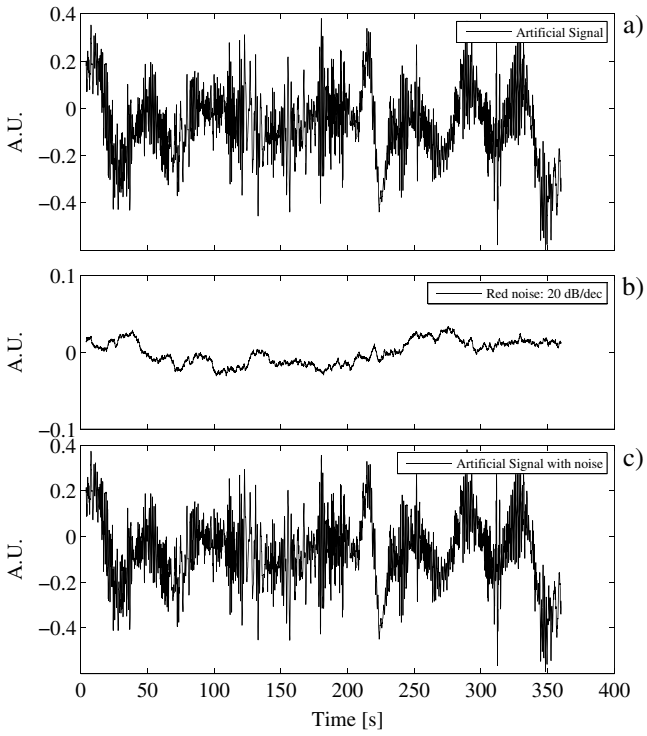

Figure 1. Artificial signal under study. (a) Artificial signal generated as superposition of seven highly nonstationary IMCs; (b) end noise of 20 dB; (c) artificial signal perturbed with red noise of 20 dB.

frequency analysis which follows from the ALIF decomposition with the ones produced by using short time Fourier transform (STFT) (Cohen, 1995) and continuous wavelet transform (CWT) (Daubechies, 1990).

Figure 1c shows the artificial signal under study, which is generated as superposition of seven highly nonstationary IMCs (Figure 1a), plus red noise (Figure 1b), in order to mimic a real-life intermittent GNSS signal, described in section 5. The shape of the seven modes of the ground truth was chosen using the following AM-FM model: we fixed the frequency to a constant value and let the amplitude vary randomly, ensuring at the same time the single-mode statistics to resemble the reference GPS signal. Concerning the red noise (Figure 1b), we used the Zhivomirov Matlab function that generated a sequence of Brownian samples (Manolakis & Ingle, 2011). Using the signal-to-noise ratio formula $\mathrm{SNR}_{\mathrm{dB}} = 20\log_{10}\frac{\sigma(\mathrm{signal})}{\sigma(\mathrm{noise})}$, valid for finitely supported sampled signals and where σ stands for standard deviation, we set the level of noise to 20 dB. This is a worst case analysis since, in real-life GNSS signals, the level of noise is at most around 20 dB (Kintner et al., 2009). We point out that the choice of a red noise perturbation of the artificial signal is, from the point of view of the ability of the algorithm to handle such signal, arbitrary. It is interesting to note that ALIF can manage any kind of noise. For instance, Cicone et al. (2016a) show that ALIF works well also in presence of heavy white noise (up to −10 dB). We decompose the proposed artificial signal using the ALIF algorithm described in section 2, the DWT summarized in the previous section, and the EEMD (Wu & Huang, 2009). The parameters chosen for the EEMD decompositions are as follows: the ratio between the standard deviation of the added noise and that of the signal was set to 0.2; the number of ensemble members was set to 100; the number of expected IMCs was set to 8.

Figure 2 shows the decomposition obtained using ALIF with constant mask length (black lines) superimposed to the components that constitutes the artificial signal (red lines). Figures 3 and 4 show the EEMD and DWT decomposition (black lines), respectively compared to the components of the artificial signal (red lines). The comparison between the IMCs and the ground truth components have been made frequency by frequency (i.e., scale by scale). It is evident that the ALIF method properly decomposes the given signal reproducing exactly the components of the ground truth with a one-to-one correspondence, as visible from each panel of Figure 2. On the contrary, in the EEMD decomposition some IMCs components do not have a clear corresponding ground truth component (we compare them with a zero signal). The second and the third EEMD IMCs, instead, correspond with the first ground truth component (the algorithm is simply splitting it into two parts), respectively. Finally, concerning the DWT, the components correspond roughly to ground truth ones and many of them to the very same ground truth components. In particular, in Figure 4, we compare the first three DWT components with the first ground component, the fourth and fifth DWT components with the second and third ground truth ones, the sixth and seventh both with the fourth, the eighth and ninth with the fifth, the tenth with the sixth, the eleventh and twelfth both with the seventh, and the thirteenth with a zero signal. From this example it is clear how ALIF is capable to separate in a meaningful way a highly nonstationary signal, even in presence of noise, whereas the other two methods encounter problems. In particular, both the EEMD and the DWT produce, in this example, components that cannot be directly associated with a ground truth one. This means that there is not the desired one-to-one correspondence between components of the ground truth and components of the EEMD/DWT decomposition. Another approach used in the analysis of a nonstationary signal is the calculation of the so-called time-frequency representation. This can be done with many techniques. The most well-known ones are the STFT and the CWT. In Figure 5 we compare such time-frequency representations with the outcome of a frequency analysis performed on each ALIF IMCs component separately. Figure 5a shows the STFT and the CWT (Figure 5b) time-frequency representation of the signal. Figure 5c displays the instantaneous frequencies over time of each ALIF IMC component computed using the new definition of instantaneous frequency proposed in Cicone et al. (2016a, equation 34). This new definition has the advantage to be completely local, whereas the standard method, based on the so-called Hilbert Transform (Huang et al., 1998), is not since it relies on an integration over the entire time domain.

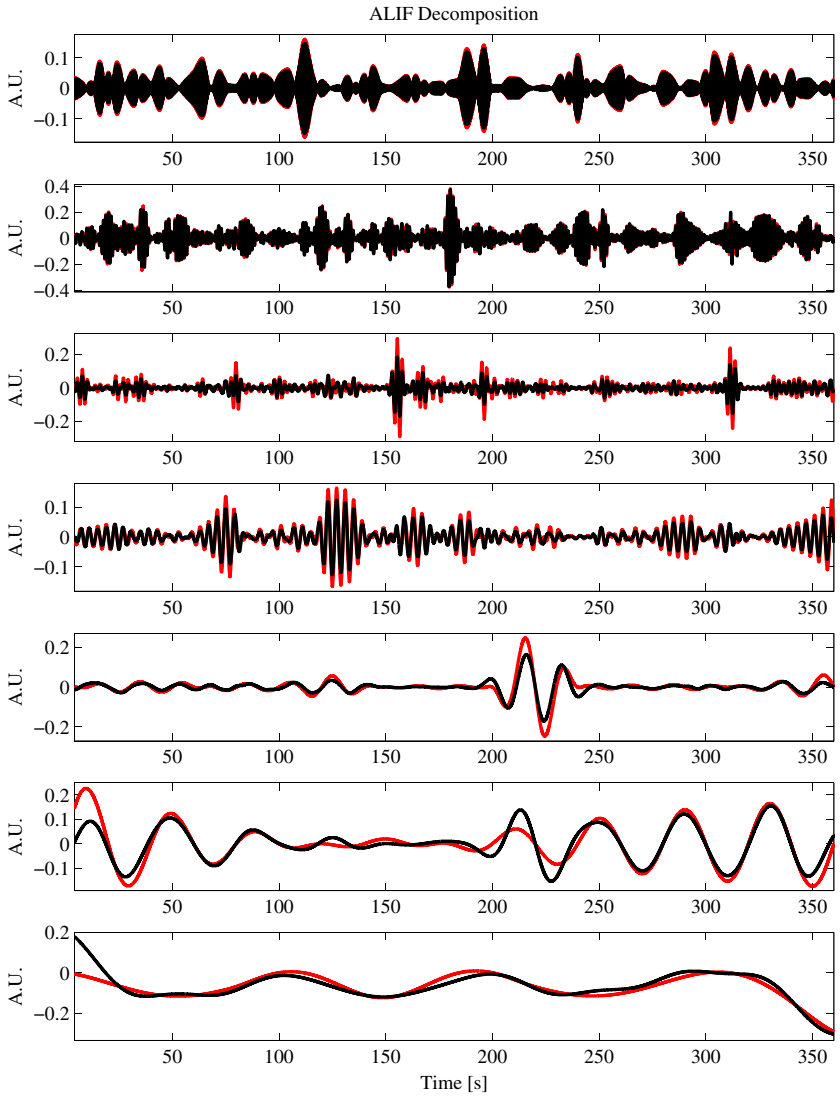

Figure 2. Superposition of the decomposition produced using ALIF with constant mask length (black) and the ground truth (red). Panels from top to bottom show the IMCs from highest to lower frequency, respectively, for both red and black lines.

From these plots it is evident that both STFT and CWT suffer from limited resolution due to the uncertainty principle studied by Cohen in 2001. Whereas, ALIF achieves a better accuracy since it first decomposes a nonstationary signal into a few simple components and then performs a component by component analysis.

In Figure 6 we report the distribution of statistical moments at different scales for the artificial signal decomposed with ALIF, DWT, and EEMD, with and without red noise. From this analysis it is clear that ALIF is able to decompose the signal into meaningful components better than EEMD and DWT, even in presence of red noise.

5. Example of Application: Ionospheric Scintillation

To provide an example of ALIF application in the space physics domain, we consider the ionospheric radio power scintillation on L band. In particular, we focused on scintillation experienced by Global Navigation Satellite System (GNSS) signals when received at ground. Specifically, time series of raw power present features common to many space physics signals, such as nonstationarity, scale-dependent statistics, intermittency, and non-Gaussianity.

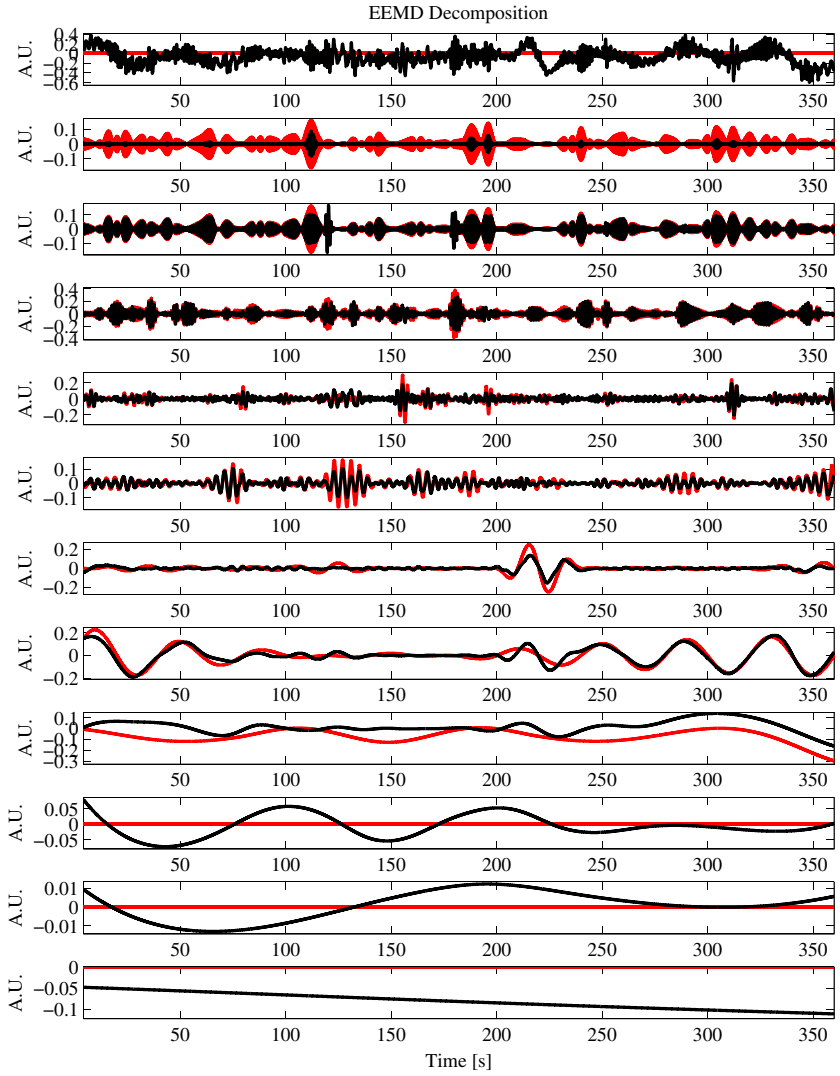

Figure 3. Superposition of the decomposition produced using EEMD (black) and the ground truth (red). Panels from top to bottom show the IMCs from highest to lower frequency, respectively, for both red and black lines.

Ionospheric radio scintillation is both *a problem and an opportunity*: on the one hand, it poses a threat on GNSS-reliant services, because it may cause the loss of lock of the signal or degradation in positioning accuracy; on the other hand, the properties of the turbulent ionospheric medium may be inferred by studying the scintillation occurrence and characteristics (Grzesiak & Wernik, 2012; Wernik et al., 1990; Wernik & Grzesiak, 2011).

Being a consequence of ionospheric turbulence, scintillation depends considerably on what determines plasma turbulence and radio propagation; hence, it is very variable with magnetic local time and satellite and receiver location. Scintillation also depends on the satellite-receiver-ionosphere relative geometry, on satellite zenith angle, and on the propagation angle with respect to the magnetic field (Aarons, 1982, 1983; Basu & Basu, 1985; Kersley et al., 1988; MacDougall, 1990a, 1990b).

A key aspect of radio scintillation is its scale-dependent behavior. In fact, if the signal is observed with different time resolution, it shows different statistical properties, depending on the small-scale properties of the ionospheric medium, as plasma turbulence occurs (Materassi et al., 2005; Materassi & Mitchell, 2007).

In general, the ionospheric diffraction index n should be described as the sum of a smooth background n_0, to which the whole n reduces when gradients and dynamics are negligible, and an irregular term δn describing small-scale fluctuations (Wernik et al., 2007):

$$n\left(\vec{x},t\right) = n_0\left(\vec{x},t\right) + \delta n\left(\vec{x},t\right). \tag{11}$$

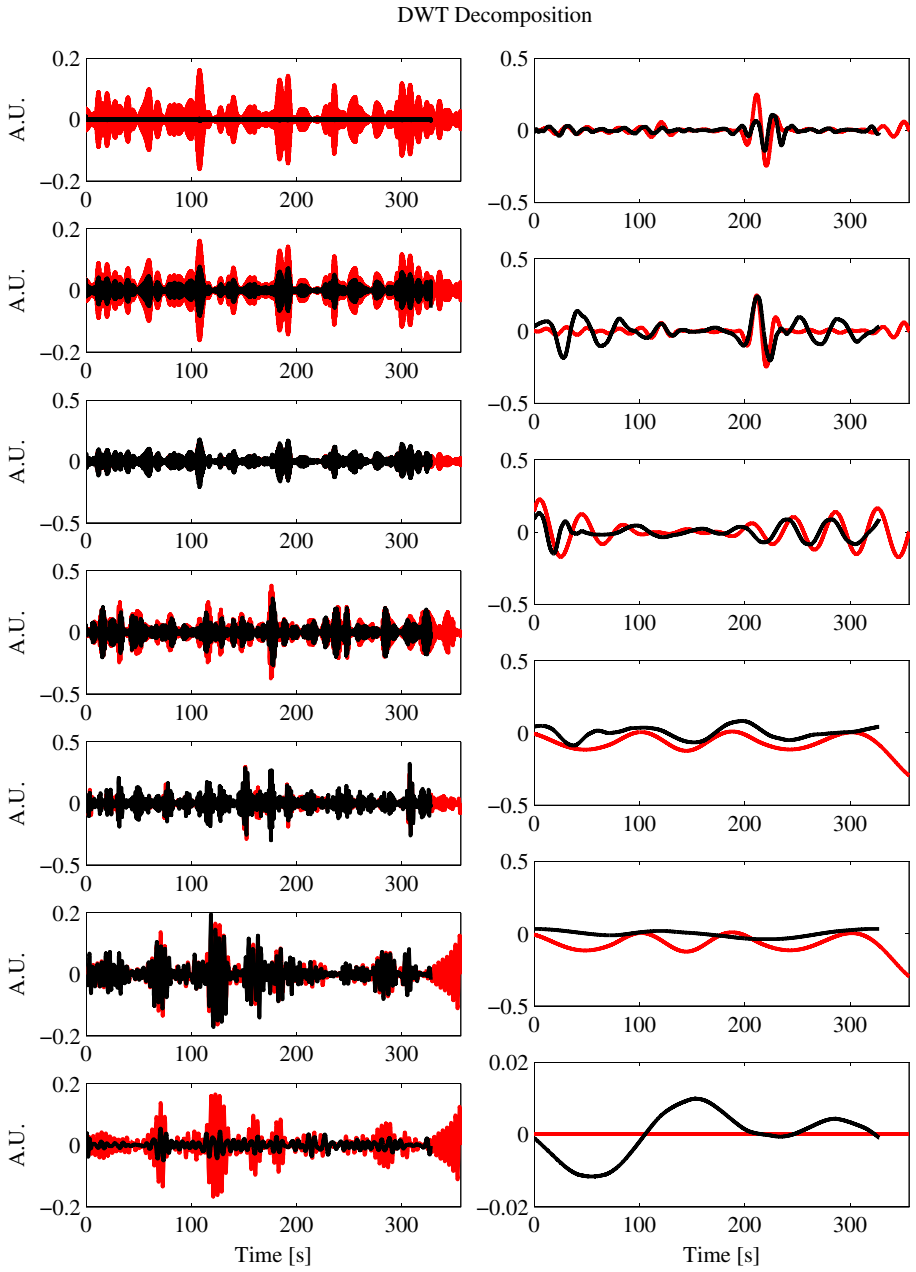

Figure 4. Superposition of the decomposition produced using DWT (black) and the ground truth (red). In each column, panels from top to bottom show the DWT components from highest to lower frequency, respectively, for both red and black lines.

Local quantities determining δn show *multifractal properties* (Yordanova et al., 2004) that depend both on the position $\vec{x}$ and the time t, and are driven by the general conditions (De Michelis et al., 2015). Such properties are handed down to the irregular, highly varying, and apparently random diffraction patterns of electromagnetic waves that cross the ionosphere, i.e., radio scintillation, that may be regarded as the signature of plasma turbulence left on the radio signal. However, it should be nontrivial to read the multiscale properties of δn out of the multiscale properties of scintillation time series (Materassi et al., 2005).

Multiscale properties discussed in the following are treated as *probabilistic*, as done in the turbulence literature (Frisch, 1995; Materassi & Consolini, 2008).

The power of a ionospheric scintillation is the radio scintillation observed on the time series $w(t)$ of the power collected by the ground receiver where $w \propto \left|\vec{E}\right|^2$, being $\vec{E}$ the electric field of the incident wave. Since this

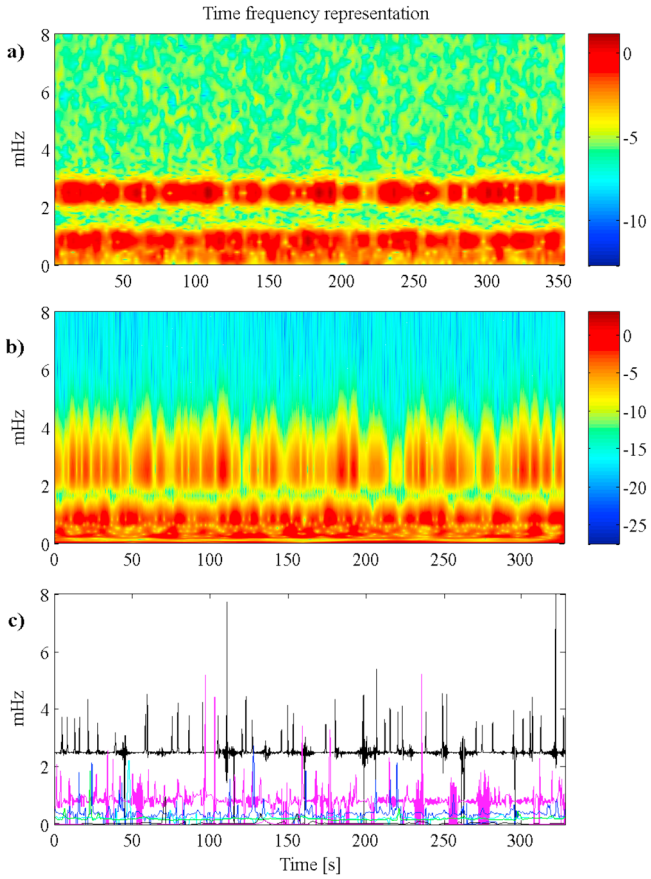

Figure 5. Time-frequency representation using (a) STFT and (b) CWT. (c) The instantaneous frequencies over time of the IMCs produced by ALIF.

field is an exponential of a linear functional of the diffraction index $n = n_0 + \delta n$ (Yeh & Liu, 1982)

$$\vec{E} = \vec{E}_0 \cdot \exp(\mathcal{L}(n_0)) \cdot \exp(\mathcal{L}(\delta n)), \tag{12}$$

then the decomposition of the $w(t)$ in low-frequency trend $w_0(t)$ and high-frequency fluctuations $w_{\text{det}}(t)$ is a factorization (Van Dierendonck et al., 1993).

$$w(t) = w_0(t) \cdot w_{\text{det}}(t), \tag{13}$$

where $w_0 \propto \exp(\mathcal{L}(n_0))$ and $w_{\text{det}} \propto \exp(\mathcal{L}(\delta n))$ (Materassi & Mitchell, 2007). The parameter w_0 includes the variability of w of geometric origin, i.e., variable satellite-receiver distance. The series $w_0(t)$ is obtained by low-pass filtering $w(t)$ (Materassi et al., 2009)

$$w_0(t) = w_{f<f_{\text{filter}}}(t),$$

so that the "detrended" signal reads

$$w_{\text{det}}(t) = \frac{w(t)}{w_{f<f_{\text{filter}}}(t)}. \tag{14}$$

The frequency f_{filter} has been selected as described in Materassi et al. (2009). Time scales in $w_{\text{det}}(t)$ correspond to space scales in δn, according to the interplay between the plasma evolution and the satellite motion (Rino, 1979a, 1979b; Yeh & Liu, 1982). Then, *the temporal characteristics of* $w_{\text{det}}(t)$ *at different time scales* are studied to investigate the *space multiscale statistical properties* of $\delta n(\vec{x})$. It is worth noting that there exists an intrinsic time variability of plasma in δn. The key assumption is that this takes place on times longer than the satellite scan, during which the medium does not change its local properties. In practice, the time dependence in $w_{\text{det}}(t)$ just results out of the motion of the satellite across the nonhomogenous medium.

In order to study its multiscale proprieties (Wernik, 1997), $w_{\text{det}}(t)$ is decomposed along functions $g_l(t)$ each of which shows a characteristic scale of variability l (*multiscale decomposition*). The statistics of the values $g_l(t)$ for the different scales l's, referred to as *statistical multiscale properties* of w_{det}, can be analyzed by evaluating: the variance $\sigma(l)$, the skewness $S(l)$, the kurtosis excess $K_{\text{ex}}(l) = K(l) - 3$, the relative energy ϵ_{rel}, and the Shannon information entropy $I(l)$. The first three parameters are the second, the third, and the fourth moment of the probability distribution $p(g_l)$ of $g_l(t)$, respectively. The ϵ_{rel} is the ratio between the square L_2 modulus of $g_l(t)$ and the total energy of the signal, that is,

$$\epsilon_{\text{rel}}(l) = \frac{\int_l |g_l(t)|^2 \, dt}{\int_l |w_{\text{det}}(t)|^2 \, dt}. \tag{15}$$

The Shannon information $I(l)$ is defined as follows:

$$I(l) = -\sum_{\{g_l\}} p(g_l) \log_2 p(g_l). \tag{16}$$

These parameters give an idea of how the statistics of the signal varies with the scale considered (Strumik & Macek, 2008). In particular, $K_{\text{ex}}(l)$ indicates how rare fluctuations are abundant at different l's: if $K_{\text{ex}}(l)$ increases as l gets smaller and smaller, the signal is defined as *intermittent* (Frisch, 1995). The ϵ_{rel} gives a measure of how "energetically strong" the l component is in the sum (16). $I(l)$ measures the "degree of randomness" attributed to the l component of the signal.

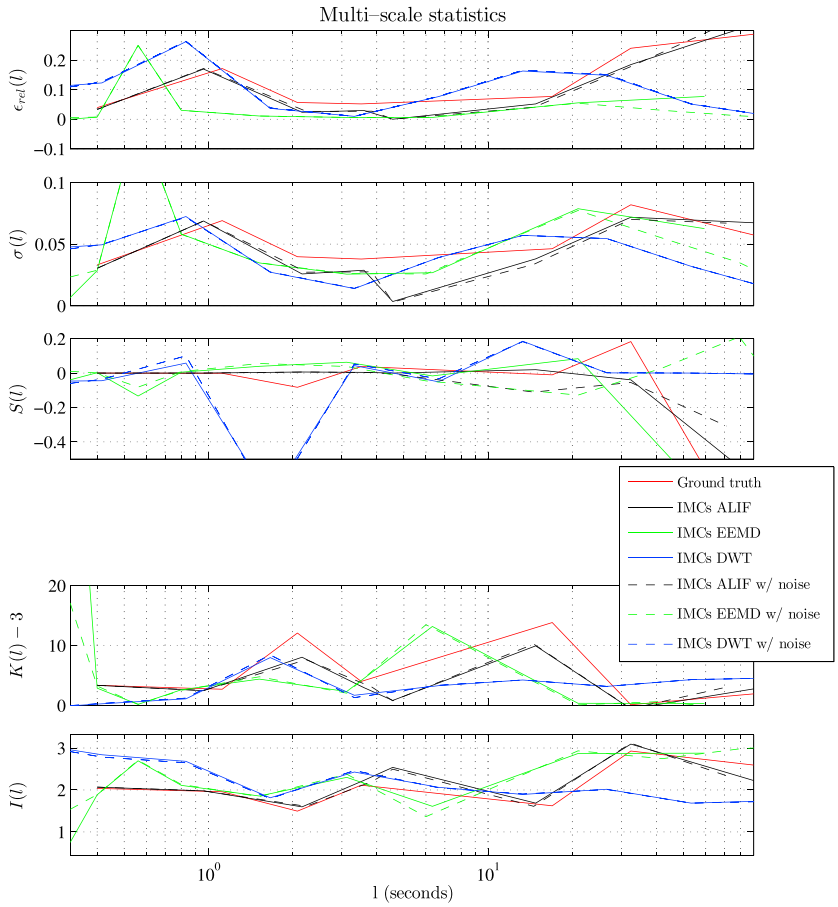

Figure 6. Multiscale statistics obtained by means of ALIF, DWT, and EEMD, with and without red noise.

5.1. Scintillation Event Analysis

Data are collected via GPS ionospheric scintillation monitor receiver (GISTM; Van Dierendonck et al., 1993) located in San Miguel de Tucumán, Argentina (26.9°S, 294.6°E) (Alfonsi et al., 2013). The GISTM is able to sample data at 50 Hz. The selected data segment refers to the following interval (named J_M): 12 March 2011; UT = 00:00.0–00:13.0 (LT = UT − 3), extracted during the recovery phase of a moderate geomagnetic storm that occurred between 10 and 16 March 2011. J_M is characterized by two clearly different regimes: low (J_L) and high (J_H) intermittency. J_L and J_H have been analyzed jointly (J_M) and separately, highlighting their different statistical proprieties as a function of the time scales. J_L corresponds to 00:00.0 < UT < 00:05.46 time interval, J_H corresponds to 00:06.0 < UT < 00:11.46 time interval, while J_M corresponds to 00:02.0 < UT < 00:12.09 time interval. To obtain the detrended signal, the highest frequency f_{filter} in (14) not altering the variance of the f-filtered signal has been chosen. This yields the statistics of the detrended signal frequency independent and removes the effects of large-scale variability caused by the relative geometry/motion between the satellite and the ionosphere (Materassi & Mitchell, 2007; Materassi et al., 2009).

The signal decomposition was made by applying both ALIF and DWT. It is important to remind here that differently from DWT, ALIF does not require signals with length exactly equal to a power of 2. Furthermore, since the signal is sampled at 50 Hz, the sampling time is $\Delta t = 2 \times 10^{-2}$ s, and in the DWT $l_m = 2^m l_{\text{min}}$, where the smallest possible scale is $l_{\text{min}} = 2\Delta t = 0.04$ s.

5.1.1. Interval J_M

Figure 7a shows the raw power along the following time interval: 12 March 2011, UT = 00:02.0–00:12.9. Apparently, the signal presents an onset of intermittency at $t_0 = \simeq 210$ s. Left panels (Figure 7b) and right panels (Figure 7c) show the statistical parameters as a function of the scale, evaluated by means of ALIF, with constant mask length and DWT, respectively. Both methods show that the signal energy is distributed according to different statistics at different scales; the signal fluctuations show different probability density

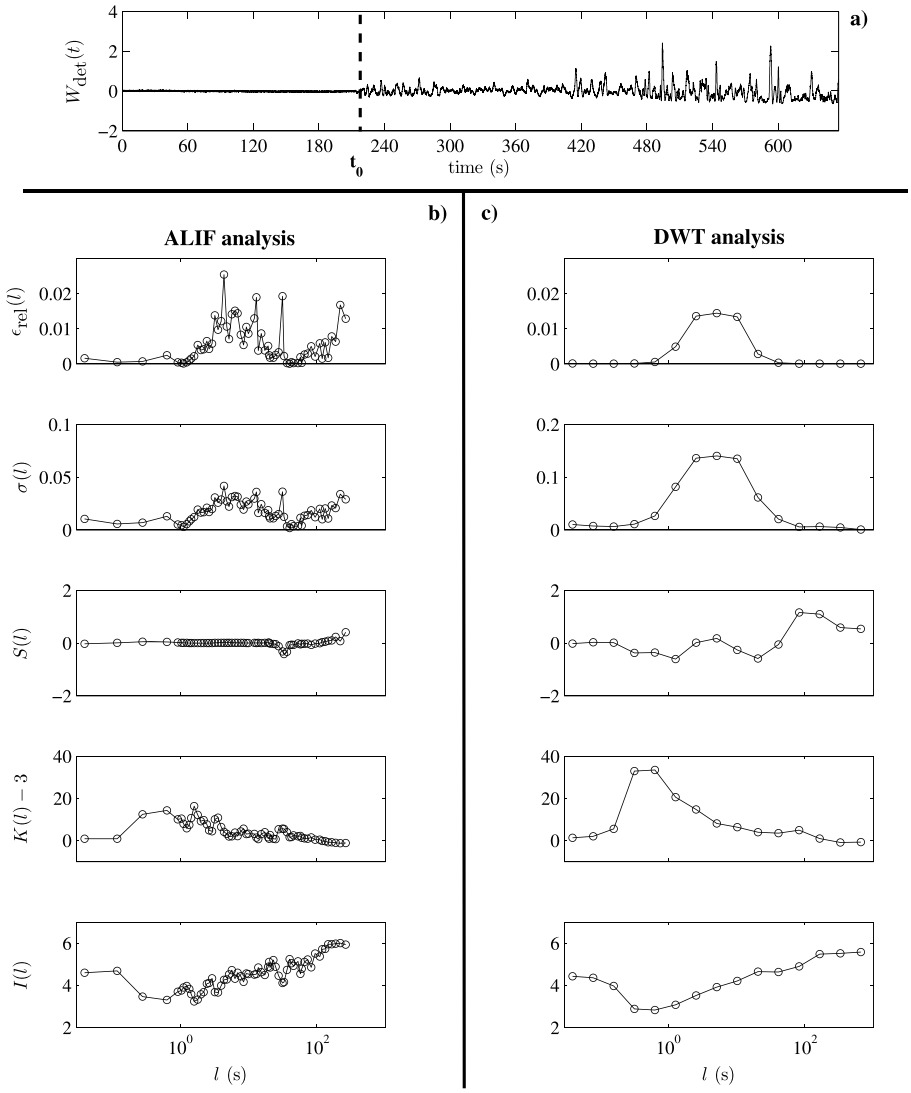

Figure 7. Multiscale statistical analysis along the time interval corresponding to J_M interval (UT = 00:02.0–00:12.9). (a) Raw power behavior as a function of time (black dashed line represents the time t_0 at which the signal changes its intermittency characteristics); (b and c) Multiscale statistical analysis by means of ALIF and DWT methods, respectively. In each box, from top to bottom, relative energy, standard deviation, skewness, excess of kurtosis, and Shannon information behaviors as functions of the scale l have been represented.

functions (PDFs) and information entropy content at different scales. In particular, it is relevant to see that the signal fluctuations are clearly not normally distributed (as evident from $K(l) - 3$) in the scale ranges 0.1–10 s. Different results are obtained for the skewness S. ALIF with constant mask length (which boils down to IF) is intended to produce modes (IMC) characterized by skewness values as close as possible to zero. S_{DWT} shows positive values as expected from the detrending technique adopted (Materassi & Mitchell, 2007). However, both methods did not highlight any clear scale dependence of the skewness.

5.1.2. Interval J_L

Figure 8a shows the low intermittency interval J_L of the signal. The signal aspect does not suggest any clear evidence of scale dependence of fluctuation statistics. In fact, the values of $K(l) - 3$, evaluated by both methods, fluctuate around zero, indicating an approximately Gaussian nature of this kind of signal independent of the scale. As a confirmation of statistical l homogeneity, $I(l)$ shows an almost monotonically slow increase from $I(l) = 5$ to $I(l) = 6$ for both ALIF, with constant mask length and DWT. A different behavior has been obtained for ϵ_{rel}, which presents decreasing values for 0.04 s < l < 0.4 s. For scales greater than 0.4 s, the energy shows

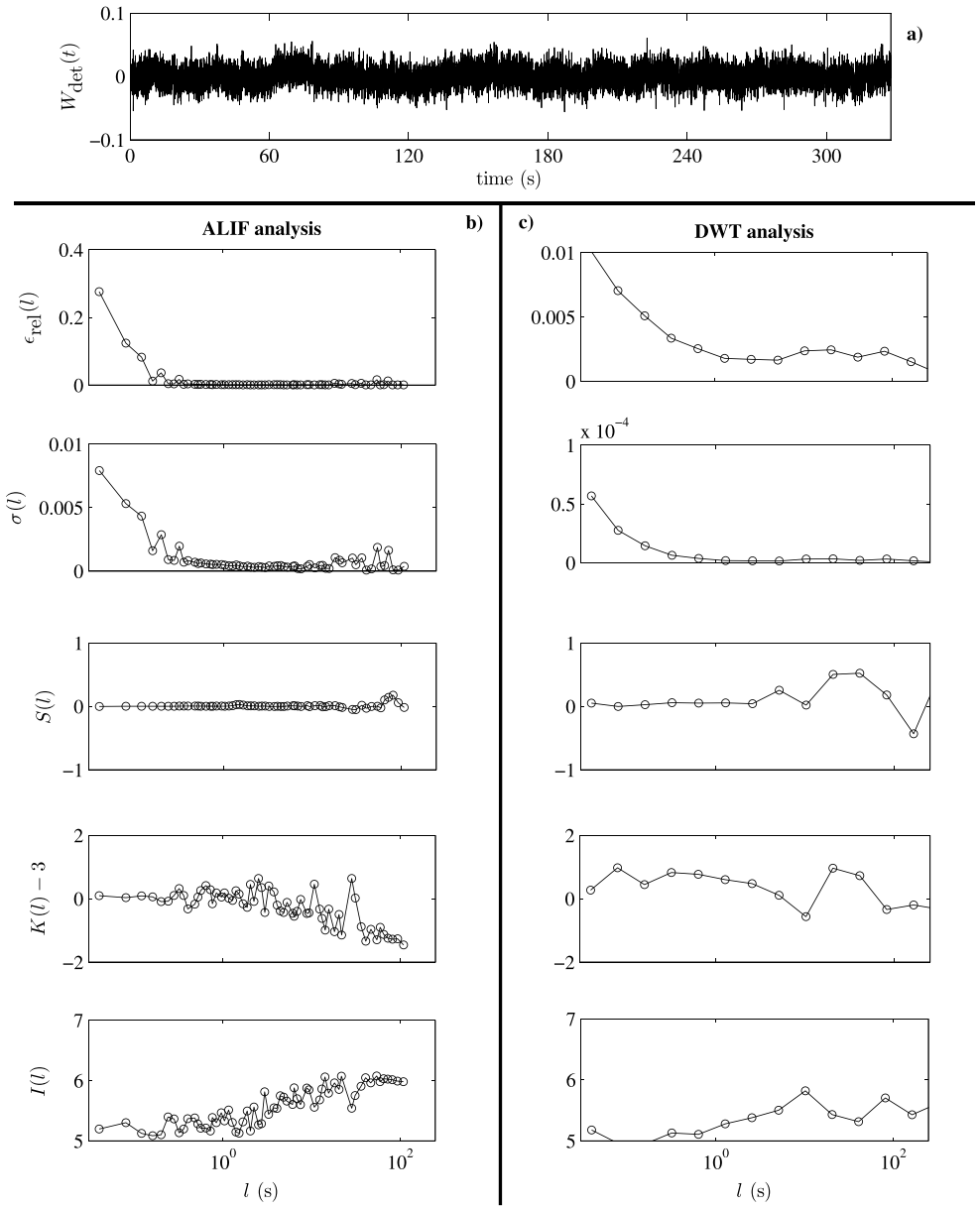

Figure 8. Multiscale statistical analysis along the time interval corresponding to the J_L interval (00:00.0 < UT < 00:05.46). (a) Raw power behavior as a function of time; (b and c) Multiscale statistical analysis by means of ALIF and DWT methods, respectively. In each box, from top to bottom, relative energy, standard deviation, skewness, excess of kurtosis, and Shannon information behaviors as functions of the scale l have been represented.

very low values. The parameter σ shows the same behavior as ϵ_{rel} for both ALIF and DWT. Both methods did not highlight any clear scale dependence of the skewness.

5.1.3. Interval J_H

Figure 9a shows the more intermittent interval J_H of the signal. A visual inspection suggests the appearance of larger fluctuations at scales higher with respect to the J_L interval. This is confirmed by the higher-energy values at scale between 1 and 30 s evaluated by both ALIF, with constant mask length (Figure 9b), and DWT (Figure 9c) methods. The same behavior has been obtained for σ, showing almost constant values for $0.04 < l < 1$ s and higher values for $l > 2$ s. In addition, either K_{ALIF} or K_{DWT} shows clear peaks at $l \sim 0.3$ s, $l \sim 1.6$ s and $l \sim 8$ s. The results obtained for the kurtosis are accompanied by the Shannon entropy behavior (I), which shows valleys corresponding to the $K - 3$ peaks. Also in this interval, both methods did not highlight any clear scale dependence of the skewness.

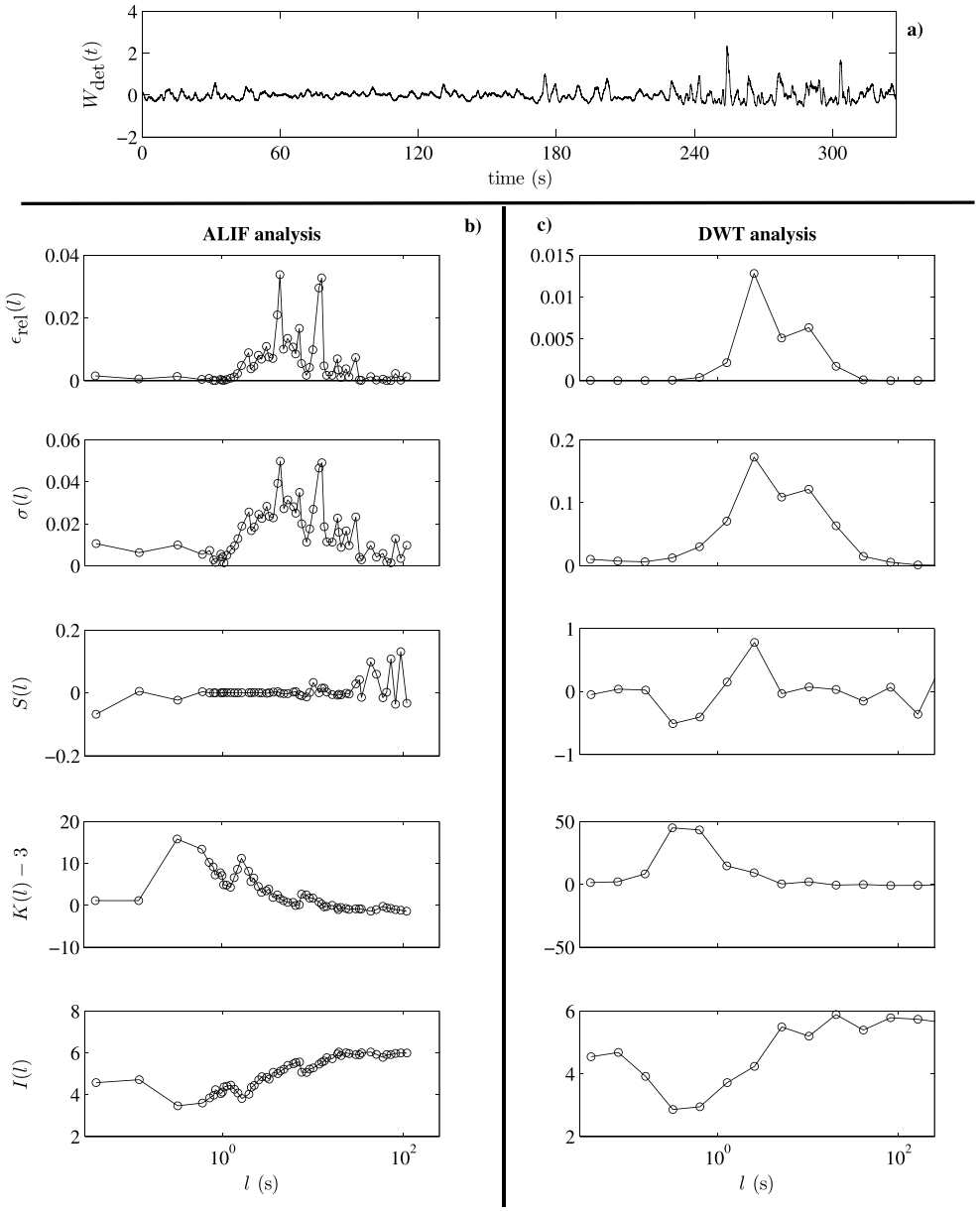

Figure 9. Multiscale statistical analysis along the time interval corresponding to the J_H interval (00:06.0 < UT < 00:11.46). (a) Raw power behavior as a function of time; (b and c) Multiscale statistical analysis by means of ALIF and DWT methods, respectively. In each box, from top to bottom, relative energy, standard deviation, skewness, excess of kurtosis, and Shannon information behaviors as functions of the scale *l* have been represented.

6. Discussion and Conclusions

This paper presents a new data analysis technique, the ALIF, which generalizes the IF method (Lin et al., 2009). The novelty introduced by ALIF is the capability of decomposing any kind of signal, in particular, nonstationary ones, into a few simple components called IMCs. Compared with standard techniques for nonstationary signals, like Wavelet transform or STFT, this method allows deriving sharper time-frequency representations and more detailed statistical proprieties of a signal. In the special case of constant mask length, ALIF reduces to IF, whose stability and convergence can be a priori guaranteed. For this reason, we preferred to show in the current paper examples of decomposition by IF. However, we underline that ALIF allows currently for an a posteriori stability and convergence analysis, which can be directly derived from the decomposition of a given signal. Furthermore, necessary and sufficient conditions for the a priori stability and convergence of ALIF are currently under investigation. In this work we tested ALIF with constant mask length against ionospheric radio power

scintillation in GNSS signal, which we decomposed and then analyzed from a statistical point of view. To detail ALIF performance, we compare its outcomes with those obtained using the classical DWT. Regarding the test example, we observe that when a signal is scale filtered, it is possible to see that its statistical proprieties depend on scale, and this dependence is different for signals with different intermittency. ALIF, with constant mask length, and DWT, in general, give consistent results about the behavior of the statistical properties as functions of the scale in different intermittency conditions. Both methods are able to distinguish between scales at which the signal appears more similar to Gaussian noise and those at which the signal is more complex and properly turbulent, that is, intermittent. In fact, the ability of both methods to decompose a nonstationary signal locally in time allows to produce an analysis much richer than a simple power versus frequency inspection as in the Fourier analysis. As an example, in the analysis of segments J_M and J_H, the Shannon entropy shows a valley around the scales of leptokurtic signal ($0.1 < l < 3$ s). According to definition (16), in this interval there is decrease of disorder in the signal. This suggests the appearance of localized structures due to turbulence (Ebeling, 1989; Klimontovich, 1995, 1996).

On the other hand, ALIF, with constant mask length, and DWT show some meaningful differences. In particular, they sample intrinsically different scales, as ALIF scales assortment is richer than the diadic one of DWT. As an example, it highlights peaks of kurtosis $K(l)$ at scales that are not visible by DWT, especially in the most turbulent/mixed segments of the signal. This makes ALIF stronger in detecting intermittency intervals. Conversely, the signal energy and the standard deviation are distributed by ALIF on a wider number of modes fixing their maxima at different values with respect to DWT. However, in DWT the signal is decomposed into *independent* components, being the functions $f_{l,\tau}$ orthogonal to each other, whereas ALIF method, as for EMD technique, does not produce orthogonal components. Nevertheless, since the so-called IMCs are produced by subsequent subtraction from the given signal of the previously computed IMCs, they are independent from a statistical point of view.

ALIF is a technique able to separate a signal into different IMCs, according to their scales. Concerning the physical meaningfulness of the IMCs, the statistical significance of ALIF revests a crucial role. In fact, Flandrin et al. (2004), Flandrin and Goncalv'es (2004), and Wu and Huang (2004, 2005) investigated how the noise can be separated satisfactorily from information on a certain data set. On the other hand, Ghil et al. (2002) applied a Monte Carlo statistical significance test to SSA (singular spectrum analysis), MEM (maximum entropy method), and MTM (multitaper method) techniques in order to establish how these methods could provide reliable results. Regarding ALIF, the development of a proper statistical test will be treated in a forthcoming paper, where several data sets will be analyzed.

Concerning the skewness, ALIF method is designed to extract modes (IMCs) whose envelopes, that is, the curves connecting its maxima and minima, are symmetric with respect to the horizontal axis. Therefore, ideally, the skewness should be constantly zero for every scale. Anyway, the iterative method requires ideally infinitely many steps to produce each IMC. In practice, in the computation, a stopping criterion is used to allow to discontinue the calculations usually after a few steps. This explains why the produced modes are not perfectly symmetric and, hence, also the reason why the skewness ends up to be not always zero. However, it can be observed that it is always possible to use the skewness values to adjust the stopping criterion in order to improve the quality of the decomposition.

Furthermore, it can be pointed out that the ALIF algorithm can be also used as a detrending technique, since it allows to separate the oscillatory parts of signal from its trend.

In conclusion ALIF method with *constant mask length* allows to describe, better than DWT, the multiscale nature of a signal. In the ionospheric scintillation case, this may lead to clarify the relationship between the small-scale time scale structure in the signal and the turbulence in the medium.

On the other hand, ALIF *with variable mask length*, even though still under study from a theoretical point of view, appears to be, by itself, a promising and more performing technique for the decomposition of nonstationary and nonlinear signals.

From a scientific point of view, the ability of ALIF to efficiently separate the different scales is useful to make a scale-by-scale comparison among solar wind (SW), magnetosphere, and ionosphere. This can be used to build new models of the SW-magnetosphere-ionosphere coupling (through multiscale coupling). In addition, ALIF allows evaluating how the SW turbulence is translated into ionospheric turbulence.

Another potential field of application is the identification of peculiar oscillation modes (e.g., on ionospheric/magnetospheric plasma density, magnetospheric sudden impulses) that switch on when an external forcing (e.g., SW) is present on a given system (Piersanti et al., 2012, 2017; Piersanti & Villante, 2016; Vellante et al., 2014; Villante & Piersanti, 2008, 2009). This follows from the capability of ALIF in disentangling regular from irregular variations on a given signal.

All these features make ALIF a promising tool to support the development of new space weather models and/or tools able to infer the magnetospheric/ionospheric behavior from direct SW observations.

Acknowledgments
Authors are grateful to Miguel Cabrera and Vincenzo Romano for the support in the installation and the maintenance of the GNSS receiver in San Miguel de Tucumán. A. Cicone was supported by the "INdAM Fellowships in Mathematics and/or Applications cofunded by Marie Curie Actions," FP7–PEOPLE–2012–COFUND, grant agreement PCOFUND–GA–2012–600198. The ALIF code is available at www.cicone.com.

References

Alfonsi, L., Spogli, L., Pezzopane, M., Romano, V., Zuccheretti, E., De Franceschi, G., & Ezquer, R. G. (2013). Comparative analysis of spread-*F* signature and GPS scintillation occurrences at Tucumán, Argentina. *Journal of Geophysical Research: Space Physics*, *118*, 4483–4502. https://doi.org/10.1002/jgra.50378

Aarons, J. (1982). Global morphology of ionospheric scintillation. *Proceedings of the IEEE*, *70*, 360–378.

Aarons, J. (1983). The longitudinal morphology of equatorial *F*-layer irregularities relevant to their occurrence. *Space Science Reviews*, *63*, 209–243.

Basu, Su., & Basu, S. (1985). Equatorial scintillations: Advances since ISEA-6. *Journal of Atmospheric and Terrestrial Physics*, *47*, 753–768.

Cicone, A., Liu, J., & Zhou, H. (2016a). Adaptive local iterative filtering for signal decomposition and instantaneous frequency analysis. *Applied and Computational Harmonic Analysis*, *41*(2), 384–411. https://doi.org/10.1016/j.acha.2016.03.001

Cicone, A., Liu, J., & Zhou, H. (2016b). Hyperspectral chemical plume detection algorithms based on multidimensional iterative filters decomposition. *Philosophical Transactions of the Royal Society of London, Series A: Mathematical, Physical and Engineering Sciences*, *374*(2065), 20150196. https://doi.org/10.1098/rsta.2015.0196

Cicone, A., & Zhou, H. (2017). Multidimensional iterative filtering method for the decomposition of high-dimensional non-stationary signals. *Numerical Mathematics: Theory, Methods and Applications*, *10*(2), 278–298. https://doi.org/10.4208/nmtma.2017.s05

Cohen, L. (1995). *Time-frequency analysis* (Vol. 778). Englewood Cliffs, NJ: Prentice Hall PTR.

Cohen, L. (2001). The Uncertainty Principle for the Short-Time Fourier Transform and Wavelet Transform. In L. Debnath (Ed.) *Wavelet transforms and time-frequency signal analysis, Applied and Numerical Harmonic Analysis*. Boston, MA: Birkhäuser.

De Michelis, P., Consolini, G., & Tozzi, R. (2015). Magnetic field fluctuation features at Swarm's altitude: A fractal approach. *Geophysical Research Letters*, *42*, 3100–3105. https://doi.org/10.1002/2015GL063603

Daubechies, I. (1990). The wavelet transform, time-frequency localization and signal analysis. *IEEE Transactions on Information Theory*, *36*(5), 961–1005.

Daubechies, I., & Maes, S. (1996). A nonlinear squeezing of the continuous wavelet transform based on auditory nerve models. In *Wavelets in Medicine and Biology* (pp. 527–546). Boca Raton, FL: CRC Press.

Daubechies, I., Lu, J., & Wu, H.-T. (2011). Synchrosqueezed wavelet transforms: An empirical mode decomposition-like tool. *Applied and Computational Harmonic Analysis*, *30*(2), 243–261.

Ebeling, Werner (1989). On the entropy of dissipative and turbulent structures. *Physica Scripta*, *T25*, 238–242.

Farge, M. (1992). Wavelet transforms and their application to turbulence. *Annual Review of Fluid Mechanics*, *24*, 395–457.

Flandrin, P. (1998). *Time-frequency/time-scale analysis* (Vol. 10). San Diego, CA: Academic Press.

Flandrin, P., Rilling, G., & Goncalv'es, P. (2004). Empirical mode decomposition as a filter bank. *IEEE Signal Processing Letters*, *11*, 112–114.

Flandrin, P., & Goncalv'es, P. (2004). Empirical mode decompositions as data-driven wavelet-like expansions. *International Journal of Wavelets, Multiresolution and Information Processing*, *2*, 477–496.

Frisch, U. (1995). *Turbulence, the Legacy of A. N. Kolmogorov*. Cambridge, UK: Cambridge University Press.

Ghil, M., Allen, M. R., Dettinger, M. D., Ide, K., Kondrashov, D., Mann, M. E., … Yiou, P. (2002). Advanced spectral methods for climatic time series. *Reviews of Geophysics*, *40*(1), 1003. https://doi.org/10.1029/2000RG000092

Gilles, J. (2013). Empirical wavelet transform. *IEEE Transactions on Signal Processing*, *61*(16), 3999–4010.

Grzesiak, M., & Wernik, A. W. (2012). *Ionospheric drifts estimated using GPS scintillation data during magnetic storm on 5–6th of April 2010.* Olsztyn, Poland: IGS Workshop 2012.

Hou, T. Y., Yan, M. P., & Wu, Z. (2009). A variant of the EMD method for multi-scale data. *Advances in Adaptive Data Analysis*, *1*(4), 483–516.

Huang, N. E., Shen, Z., Long, S. R., Wu, M. C., Shih, H. H., Zheng, Q., … Liu, H. H. (1998). The empirical mode decomposition and the hilbert spectrum for nonlinear and non-stationary time series analysis. *Proceedings of the Royal Society of London. Series A*, *454*(1971), 903–995.

Lin, L., Wang, Y., & Zhou, H. (2009). Iterative filtering as an alternative algorithm for empirical mode decomposition. *Advances in Adaptive Data Analysis*, *1*(4), 543–560.

Kersley, L., Pryse, S. E., & Wheadon, N. S. (1988). Amplitude and phase scintillation at high latitudes over northern Europe. *Radio Science*, *23*, 320–330.

Kintner, P. M., Humphreys, T., & Hinks, J. (2009). GNSS and ionospheric scintillation—How to survive the next solar maximum. *Inside GNSS*, 22–30.

Klimontovich, Yu. L. (1995). Criteria of self-organization. *Chaos, Solitons and Fractals*, *5*(10), 1985–2002.

Klimontovich, Y. L. (1996). Is turbulent motion chaos or order? Is the hydrodynamic or the kinetic description of turbulent motion more natural? *Physica B: Condensed Matter*, *228*(1–2), 51–62.

MacDougall, J. W. (1990a). Distribution of irregularities in the northern polar region determined from HILAT observations. *Radio Science*, *25*, 115–124.

MacDougall, J. W. (1990b). The polar-cap scintillation zone. *Journal of Geomagnetism and Geoelectricity*, *42*, 777–788.

Mallat, S. (1998). *A wavelet tour of signal processing*. New York: Academic Press.

Manolakis, D., & Ingle, V. (2011). *Applied digital signal processing*. Cambridge: Cambridge University Press.

Materassi, M., Alfonsi, L., De Franceschi, G., Mitchell, C. N., Romano, V., Spalla, P., … Yordanova, E. (2005). Intermittency and ionospheric scintillations in GPS data. In A. H. Siddiqi, et al. (Eds.), *Proceedings of the international workshop on applications of wavelets to real world problems (IWW2005), 17–18 July 2005, Istanbul (Turkey)*. Istanbul: Istanbul Commerce University Publications.

Materassi, M., & Mitchell, C. N. (2007). Wavelet analysis of GPS amplitude scintillation: A case study. *Radio Science*, *42*, RS1004. https://doi.org/10.1029/2005RS003415

Materassi, M., & Consolini, G. (2008). Turning the resistive MHD into a stochastic field theory. *Nonlinear Processes in Geophysics*, *15*(4), 701–709.
Materassi, M., Alfonsi, L., De Franceschi, G., Romano, V., Mitchell, C., & Spalla, P. (2009). Detrend effect on the scalograms of GPS power scintillation. *Advances in Space Research*, *43*(11), 1740–1748.
Piersanti, M., Villante, U., Waters, C., & Coco, I. (2012). The 8 June 2000 ULF wave activity: A case study. *Journal of Geophysical Research*, *117*, A02204. https://doi.org/10.1029/2011JA016857
Piersanti, M., & Villante, U. (2016). On the discrimination between magnetospheric and ionospheric contributions on the ground manifestation of sudden impulses. *Journal of Geophysical Research: Space Physics*, *121*, 6674–6691. https://doi.org/10.1002/2015JA021666
Piersanti, M., Cesaroni, C., Spogli, L., & Alberti, T. (2017). Does TEC react to a sudden impulse as a whole? The 2015 Saint Patrick's day storm event. *Advances in Space Research*, *60*(8), 1807–1816. https://doi.org/10.1016/j.asr.2017.01.021
Rino, C. L. (1979a). A power law phase screen model for ionospheric scintillation: 1. Weak scatter. *Radio Science*, *14*(6), 1135–1145.
Rino, C. L. (1979b). A power law phase screen model for ionospheric scintillation: 2. Strong scatter. *Radio Science*, *14*(6), 1147–1155.
Strumik, M., & Macek, W. M. (2008). Testing for Markovian character and modeling of intermittency in solar wind turbulence. *Physical Review E: Statistical, Nonlinear, and Soft Matter Physics*, *78*, 026414.
Thakur, G., & Wu, H.-T. (2011). Synchrosqueezing-based recovery of instantaneous frequency from nonuniform samples. *SIAM Journal on Mathematical Analysis*, *43*(5), 2078–2095.
Uritsky, V. M., Slavin, J. A., Khazanov, G. V., Donovan, E. F., Boardsen, S. A., Anderson, B. J., & Korth, H. (2011). Kinetic scale magnetic turbulence and finite Larmor radius effects at Mercury. *Journal of Geophysical Research*, *116*, A09236. https://doi.org/10.1029/2011JA016744
Van den Berg, J. C. (1999). *Wavelets in Physics*. Cambridge, Great Britain: Cambridge University Press.
Van Dierendonck, A. J., Klobuchar, J., & Hua, Q. (1993). Ionospheric scintillation monitoring using commercial single frequency C/A code receivers (Paper presented at the 6th International Technical Meeting (ION GPS-93)), Satellite Division of the Institute of Navigation, Salt Lake City, Utah, 22 – 24 Sept.
Vellante, M., Piersanti, M., Heilig, B., Reda, J., & Corpo, A. D. (2014). Magnetospheric plasmadensity inferred from field line resonances: Effects of usingdifferent magnetic field models. In *General Assembly and Scientific Symposium (URSI GASS), 2014 XXXIth URSI*. Beijing, China: IEEE. https://doi.org/10.1109/URSIGASS.2014.6929941
Villante, U., & Piersanti, M. (2008). An analysis of sudden impulses at geosynchronous orbit. *Journal of Geophysical Research*, *113*, A08213. https://doi.org/10.1029/2008JA013028
Villante, U., & Piersanti, M. (2009). Analysis of geomagneticsudden impulses at low latitudes. *Journal of Geophysical Research*, *114*, A06209. https://doi.org/10.1029/2008JA013920
Wernik, A. W. (1997). Wavelet transform of nonstationary ionospheric scintillation. *Acta Geophysics Polonica*, *XLV*, 237–253.
Wernik, A. W., Liu, C. H., Franke, S. J., & Gola, M. (1990). High-latitude irregularity spectra deduced from scintillation measurements. *Radio Science*, *25*(5), 883–895.
Wernik, A. W., Alfonsi, L., & Materassi, M. (2007). Scintillation modeling using in situ data. *Radio Science*, *42*, RS1002. https://doi.org/10.1029/2006RS003512
Wernik, A. W., & Grzesiak, M. (2011). Scintillation caused by the ionosphere with non-Gaussian statistics of irregularities. *Radio Science*, *46*, RS6011. https://doi.org/10.1029/2011RS004716
Wang, Y., & Zhou, Z. (2013). On the convergence of iterative filtering empirical mode decomposition. *Excursions in Harmonic Analysis*, *2*, 157–172.
Wu, Z., & Huang, N. E. (2004). A study of the characteristics of white noise using the empirical mode decomposition method. *Proceedings of the Royal Society of London Series A*, *460*, 1597–1611.
Wu, Z. H., & Huang, N. (2005). Statistical significance test of intrinsic mode functions. In N. E. Huang & S. S. P. Shen (Eds.), *Hilbert-Huang Transform and its application* (pp. 107–127). Singapore: World Scientific.
Wu, Z., & Huang, N. E. (2009). Ensemble empirical mode decomposition: A noise-assisted data analysis method. *Advances in Adaptive Data Analysis*, *1*(1), 1–41.
Yeh, K. C., & Liu, C-H. (1982). Radio wave scintillations in the ionosphere. *Proceedings of the IEEE*, *70*(4), 324–360.
Yordanova, E., Grzesiak, M., Wernik, A. W., Popielawska, B., & Stasiewicz, K. (2004). Multifractal structure of turbulence in the magnetospheric cusp. *Annales Geophysicae*, *22*, 2431–2440.